

Increasing Solar Absorption for Photocatalysis with Black Hydrogenated Titanium Dioxide Nanocrystals

Xiaobo Chen,^{1,2} Lei Liu,³ Peter Y. Yu,³ Samuel S. Mao^{1,2*}

¹Lawrence Berkeley National Laboratory, University of California at Berkeley, Berkeley, CA 94720, USA. ²Department of Mechanical Engineering, University of California at Berkeley, Berkeley, CA 94720, USA. ³Department of Physics, University of California at Berkeley, Berkeley, CA 94720, USA.

*To whom correspondence should be addressed. E-mail: ssmao@lbl.gov

When used as a photocatalyst, titanium dioxide (TiO₂) absorbs only ultraviolet (UV) light, and several approaches, including the use of dopants such as nitrogen, have been taken to narrow the band gap of TiO₂. We demonstrate a conceptually different approach to enhancing solar absorption by introducing disorder in the surface layers of nanophase TiO₂ through hydrogenation. We show that disorder-engineered TiO₂ nanocrystals exhibit substantial solar-driven photocatalytic activities, including the photo-oxidation of organic molecules in water and producing hydrogen with the use of sacrificial donor.

The effectiveness of solar-driven photocatalytic processes underlying hydrogen production and water de-contamination is dictated to a great extent by the semiconductor's capability of absorbing visible and infrared light, as well as its ability to suppress rapid combination of photo-generated electrons and holes. Nanophase TiO₂, which has a large surface area that can facilitate a fast rate of surface reactions, is a widely used wide band gap semiconductor photocatalyst for a variety of solar-driven clean energy and environmental technologies (1–4). In order to increase the limited optical absorption of TiO₂ under sunlight, there have been persistent efforts to vary the chemical composition of TiO₂ by adding controlled metal (5, 6) or non-metal (7–10) impurities that generate donor or acceptor states in the band gap. Different from impurity incorporation, self-doping that produces Ti³⁺ species in TiO₂ has also been demonstrated (11). Through doping, the solar absorption characteristics of TiO₂ have been improved to some extent. For example, when non-metallic light-element dopants are introduced (9), optical absorption of TiO₂ can be modified as the result of electronic transitions from the dopant 2*p* or 3*p* orbitals to the Ti 3*d* orbitals. At present, nitrogen-doped TiO₂ exhibits the greatest optical response to solar radiation (3), but its absorption in the visible and infrared remains insufficient.

We developed an alternative approach to improving visible and infrared optical absorption by engineering the disorder of nanophase TiO₂ with simultaneous dopant incorporation. In

its simplest form, a disorder-engineered nanophase TiO₂ consists of two phases; a crystalline TiO₂ quantum dot or nanocrystal as core, and a highly disordered surface layer where dopants are introduced (Fig. 1A). While an ensemble of nanocrystals retains the benefits of crystalline TiO₂ quantum structures for photocatalytic processes, the introduction of disorder and dopant at their surface would enhance visible and infrared absorption plus the additional benefit of carrier trapping. Large amount of lattice disorder in semiconductors could yield mid-gap states whose energy distributions differ from that of a single defect in a crystal. For example, instead of forming discrete donor states near the conduction band edge, these mid-gap states can form a continuum extending to and overlapping with the conduction band edge, thus they are often also known as band tail states. Similarly large amount of disorder can result in band tail states merging with the valence band (12–15). These extended energy states, in combination with energy levels produced by dopants, can become the dominant centers for optical excitation and relaxation. An additional potential advantage of these engineered disorders is that they provide trapping sites for photo-generated carriers and prevent them from rapid recombination, thus promoting electron transfer and photocatalytic reactions. The density of states (DOS) of disorder-engineered semiconductor nanocrystals, as compared to those of unmodified nanocrystals, is shown schematically in Fig. 1A.

To introduce disorders into nanophase TiO₂ with simultaneous dopant addition, we generated a porous network of TiO₂ nanocrystals, a few nanometers in diameter. Hydrogenation of this material creates a disordered layer on the nanocrystal surface. We observed a shift in the onset of absorption in such disorder-engineered TiO₂ nanocrystals, from the UV to near infrared after hydrogenation, accompanied by a dramatic color change and substantial enhancement in solar-driven photocatalytic activity. A photo of disorder-engineered black TiO₂ nanocrystals as compared

to that of unmodified white TiO₂ nanocrystals is shown in Fig. 1B.

We prepared TiO₂ nanocrystals with a precursor solution consisting of titanium tetraisopropoxide (TTIP), ethanol, hydrochloric acid (HCl), deionized water, and an organic template, Pluronic F127, with molar ratios of TTIP/F127/HCl/H₂O/ethanol at 1:0.005:0.5:15:40. The solution was heated at 40 °C for 24 hours, and then evaporated and dried at 110 °C for 24 hours. The dried powders were calcinated at 500 °C for 6 hours to remove the organic template and enhance crystallization of TiO₂. Both the temperature ramp rate and the cooling rate were approximately 0.3 °C per minute. The resulting white-colored powders were first maintained in a vacuum for 1 hour after placed in the sample chamber of a Hy-Energy PCTPro high-pressure hydrogen system, and then hydrogenated in a 20.0 bar H₂ atmosphere at about 200 °C for 5 days. Since hydrogen tends to be attracted to dangling bonds, we expect that the concentration of hydrogen to be the highest in the disordered layer, where there are significantly more dangling bonds than in the crystalline core of black TiO₂ nanoparticles.

We investigated the structures of the TiO₂ nanocrystals before and after hydrogenation with x-ray diffraction (XRD), Raman spectroscopy, and scanning and transmission electron microscopy (SEM and TEM). The pure TiO₂ nanocrystals are highly crystallized, as seen from the well-resolved lattice features shown in the high-resolution TEM (HRTEM) image (Fig. 1C); the size of individual TiO₂ nanocrystals is approximately 8 nm in diameter. After hydrogenation, however, the surfaces of TiO₂ nanocrystals became disordered (Fig. 1D), where the disordered outer layer surrounding a crystalline core is ~1 nm in thickness. Strong XRD diffraction peaks (Fig. 1E) also indicate that TiO₂ nanocrystals are highly crystallized. The crystalline phase has an anatase structure with an average crystal size approximately 8 nm, in agreement with HRTEM observation.

We used Raman spectroscopy to examine structural changes of the TiO₂ nanocrystals after disorder introduction with hydrogenation. The three polymorphs of TiO₂ belong to different space groups, $D_{4h}^{19}(I4_1/amd)$ for anatase, $D_{2h}^{15}(pbca)$ for brookite, and $D_{4h}^{14}(P4_2/mnm)$ for rutile, which have distinctive characteristics in Raman spectra. For anatase TiO₂, there are six Raman-active modes with frequencies at 144, 197, 399, 515, 519 (superimposed with the 515 cm⁻¹ band), and 639 cm⁻¹, respectively (3). The un-modified white TiO₂ nanocrystals display the typical anatase Raman bands, but new bands at 246.9, 294.2, 352.9, 690.1, 765.5, 849.1 and 938.3 cm⁻¹ emerge for the black TiO₂ nanocrystals, in addition to the broadening of the anatase Raman peaks (Fig. 1F). These Raman bands cannot be assigned to any of the three polymorphs of TiO₂, which indicate that structural changes occur after hydrogenation, resulting in disorders that

can activate zone-edge and otherwise Raman forbidden modes (such as modes that are IR-active only) by breaking down the Raman selection rule (13).

Solar-driven photocatalytic activity of the disorder-engineered black TiO₂ nanocrystals was measured by monitoring the change in optical absorption of a methylene blue solution at ~660 nm during its photocatalytic decomposition process. Other than being a nitrogenous reference compound for evaluating photocatalysts, methylene blue can be found as a water contaminant from dyeing processes. In a typical experiment, 0.15 mg black TiO₂ nanocrystals was added to a 3.0 ml methylene blue solution that has an optical density (O.D.) of approximately 1.0 under aerobic conditions; the results were corrected for methylene blue degradation in the absence of any photocatalyst (see SOM and fig. S1). Photodegradation was complete after 8 min for the black TiO₂ nanocrystals, whereas for the unmodified white TiO₂ nanocrystals under the same testing conditions, it took nearly 1 hour (Fig. 2A). Similar improvement was also observed for photocatalytic decomposition of phenol (see SOM and fig. S2).

The results of cycling tests of the solar-driven photocatalytic activity of black TiO₂ nanocrystals in decomposing methylene blue are shown in Fig. 2B. Once the photocatalytic reaction of a testing cycle was complete, the subsequent cycle was started after an amount of concentrated methylene blue compound was added to make the O.D. of the solution approximately 1.0. The disorder-engineered black TiO₂ nanocrystals do not exhibit any reduction of their photocatalytic activity under solar irradiation after eight photocatalysis cycles.

The disorder-engineered black TiO₂ nanocrystals exhibit substantial activity and stability in photocatalytic production of hydrogen from water under sunlight. Hydrogen gas evolution as a function of time during a 22-day testing period of solar hydrogen production experiments using black TiO₂ nanocrystals as the photocatalysts is shown in Fig. 2C. The full spectrum solar simulator was used as the excitation source, which produces about 1 sun power at the sample consisting of black TiO₂ nanocrystals loaded with 0.6 wt% Pt, placed in a Pyrex glass container filled with 1:1 water-methanol solution. (methanol is the sacrificial reagent and the anodic reaction generating O₂ from H₂O is not occurring in this system). Measurements were conducted initially for 15 consecutive days; each day the sample was irradiated for 5 hours, and then stored in darkness overnight before testing the next day. We found that 1 hour of solar irradiation generated 0.2 ± 0.02 mmol of H₂ using 0.02 grams of disorder-engineered black TiO₂ nanocrystals (10 mmol per hour per gram of photocatalysts). This H₂ production rate is about two orders of magnitude greater than the yields of most semiconductor photocatalysts (2, 16). The energy conversion

efficiency for solar hydrogen production, defined as the ratio between the energy of solar-produced hydrogen and the energy of the incident sunlight, reaches 24% for disorder-engineered black TiO₂ nanocrystals.

After testing for 13 days, 30 ml pure water was added to compensate for the loss and measurements continued for two additional days before the sample was stored in darkness for 2 days (days 16 & 17) without measurements. Experiments were resumed for 5 more days after the 2-day storage period and similar rates of H₂ evolution were still observed. Throughout the testing cycles, the disorder-engineered black TiO₂ nanocrystals exhibit persistent high H₂ production capability. Under the same experimental conditions, no H₂ gas was detected from the unmodified white TiO₂ nanocrystals loaded with Pt. We performed experiments to quantify the amount of hydrogen absorbed in black TiO₂ photocatalysts (see SOM and fig. S3). The 20.0 mg of black TiO₂ photocatalysts that were used to generate 40 mg of H₂ in 100 hours only contained about 0.05 mg of H₂. The black TiO₂ photocatalysts do not act as a hydrogen reservoir in these experiments.

We also measured photocatalytic H₂ production using black TiO₂ as the photocatalyst with only visible and infrared light by filtering out incident light with wavelengths shorter than about 400 nm. The rate of H₂ production dropped to 0.1 mmol \pm 0.02 per hour per gram of photocatalysts, reflecting the activity of the extended tail or mid-gap states of the thin disordered layer that have a narrower band gap created by disordering. We examined the change of surface chemical bonding of TiO₂ nanocrystals induced by hydrogenation with X-ray photoelectron spectroscopy (XPS) using a Physical Electronics PHI 5400 system. The Ti 2p XPS spectra were almost identical for both the white and black TiO₂ nanocrystals (see SOM and figs. S4 and S5), which indicates that Ti atoms have a similar bonding environment after hydrogenation and do not resemble spectra of TiO₂ doped with carbon or other impurities (3, 7–10). The O 1s XPS spectra of the white and black TiO₂ nanocrystals show dramatic differences (Fig. 3A), the single O 1s peak at 530.0 eV, typical for white TiO₂ can be resolved into two peaks at about 530.0 and 530.9 eV for the black TiO₂ nanocrystals. The broader peak at 530.9 eV can be attributed to Ti-OH species (17). Diffusive reflectance and absorbance spectroscopy (Fig. 3B) revealed that the band gap of the unmodified white TiO₂ nanocrystals is approximately 3.30 eV, slightly greater than that of bulk anatase TiO₂. The onset of optical absorption of the black hydrogenated TiO₂ nanocrystals was lowered to about 1.0 eV (\sim 1200 nm). An abrupt change in both the reflectance and absorbance spectra at approximately 1.54 eV (806.8 nm) suggests that the optical gap of the black TiO₂ nanocrystals is significantly narrowed by intraband transitions. No color change was observed for

the black TiO₂ nanocrystals over 1 year after they were synthesized.

The density-of-states (DOS) of the valence band of TiO₂ nanocrystals was also measured by valence band XPS (Fig. 3C). The white TiO₂ nanocrystals display typical valence band DOS characteristics of TiO₂ with the edge of the maximum energy at about 1.26 eV. Because the band gap of the white TiO₂ is 3.30 eV from the optical absorption spectrum, the conduction band minimum would occur at about -2.04 eV. For the black TiO₂ nanocrystals, the valence band maximum energy blue-shifts toward the vacuum level at approximately -0.92 eV. Combined with the results from optical measurements that suggest a much narrowed band gap, the conduction band DOS of the black TiO₂ nanocrystals would not have as significant change. Nevertheless, there may be conduction band tail states arising from disorder that extend below the conduction band minimum. Optical transitions from the blue-shifted valence band edge to these band tail states are presumably responsible for optical absorption onset around 1.0 eV in black TiO₂. A schematic illustration of the DOS of disorder-engineered black TiO₂ nanocrystals is shown in Fig. 3D.

To understand the origin of the change in the electronic and optical properties of black TiO₂ nanocrystals, we calculated the energy band structures using a first-principles density-functional theory (DFT) (18–20). Existing models of modified TiO₂ are focused on point defects, which tend to produce shallow or deep energy levels near the conduction band minimum with typical Ti³⁺ state characteristics (21–23). We studied on lattice disorders in TiO₂ nanocrystals in the presence of hydrogen and found that, rather than generating levels near the conduction band minimum, disorder-induced mid-gap states can up-shift the valence band edge of TiO₂ nanocrystals.

We first constructed a network of TiO₂ nanocrystals without disorder, but with fully relaxed surface dangling bonds. From the calculated total and projected DOS (see SOM and fig. S6), we found that the primary effect of surface reconstruction in TiO₂ nanocrystals is to produce strong band tailing near the valence band edge. The valence and conduction states are derived mainly from the O 2p orbitals and the Ti 3d orbitals, respectively. Without the introduction of disorder, we examined the band structures of TiO₂ nanocrystals containing four types of intrinsic defects with low formation energies: Ti vacancy (V_{Ti}), O vacancy (V_O), interstitial titanium (I_{Ti}), and interstitial oxygen (I_O), and three types of hydrogen impurities: interstitial H atom (I_H), interstitial H₂ molecule (I_{H2}), and H atom forming surface OH bonds with oxygen (OH_{surface}). The three native defects, V_{Ti}, V_O, and I_O, do not introduce mid-gap states, which agrees with previous calculations (24). Similarly, no mid-gap states were produced as the result of the defects associated with

hydrogen impurities (22, 23). Based on the established density functional theory (21), without disorder, the only defect that could yield a gap state in TiO₂ nanocrystals, about 0.5 eV below the conduction band minimum, is the interstitial Ti atom, I_{Ti}.

When we introduced lattice disorders in hydrogenated anatase TiO₂ nanocrystals, mid-gap electronic states were created accompanied by a reduced band gap. The disordered TiO₂ nanocrystal model, in which one H atom is bonded to an O atom while another H atom is bonded to a Ti atom, yields electronic band structures consistent with the valence band XPS measurements. A schematic illustration of a supercell of the disordered TiO₂ nanocrystal model as compared to that of a bulk anatase TiO₂ crystal is shown in Fig. 4A, and Fig. 4B plots the calculated DOS of the disorder-engineered TiO₂ nanocrystals along with those of the bulk and the unmodified TiO₂ nanocrystals. Two groups of mid-gap states (centered at about 1.8 and 3.0 eV) can be observed in the DOS of the disordered TiO₂ nanocrystals, for which the Fermi level was found to locate slightly below 2.0 eV. The different nature of these two groups of mid-gap states is revealed by the calculated partial DOS (Fig. 4C). Whereas the higher energy mid-gap states (~3.0 eV) are derived from the Ti 3d orbitals only, the lower energy states (~1.8 eV) are hybridized from both O 2p orbitals and Ti 3d orbitals, and mainly from the valence band states as the result of disorders stabilized by hydrogen. Interestingly, the hydrogen 1s orbital coupling to the Ti atom does not make significant contribution to either state, which suggests that lattice disorder accounts for the mid-gap states; hydrogen may have stabilized the lattice disorders by passivating their dangling bonds. As the lower energy mid-gap states lie below the Fermi level, they can account for a large blue shift of the valence band edge.

We also examined the 3D charge density distribution of the mid-gap electronic states (Fig. 4D) of disorder-engineered TiO₂ nanocrystals. Charges associated with the lower energy mid-gap states distribute around every O or Ti atom are indicative of the overall impact of the disorder. Because the lower energy mid-gap states are derived from hybridized O 2p orbital with the Ti 3d orbital, optical transition between these mid-gap states and the conduction band tail would produce charge transfer from the O 2p orbital to the Ti 3d orbital similar to the transition from the valence to the conduction band of bulk TiO₂. The localization of both photo-excited electrons and holes prevents fast recombination and presumably is the reason why disorder-engineered black TiO₂ can harvest more efficiently the infrared photons for photocatalysis than what bulk anatase can do to the above band gap UV photons.

References and Notes

- Grätzel, M., Photoelectrochemical cells. *Nature* **414**, 338 (2001).
- Chen, X., Shen, S., Guo, L., & Mao, S. S., Semiconductor-based photocatalytic hydrogen generation. *Chem. Rev.* **110**, 6503 (2010).
- Chen, X. & Mao, S. S., Titanium dioxide nanomaterials: Synthesis, properties, modifications, and applications. *Chem. Rev.* **107**, 2891 (2007).
- Fujishima, A., Zhang, X. & Tryk, A. D., TiO₂ photocatalysis and related surface phenomena. *Surf. Sci. Rep.* **63**, 515 (2008).
- Hoffmann, M. R., et al. Environmental Applications of semiconductor photocatalysis. *Chem. Rev.* **95**, 69 (1995).
- Choi, W., Termin, A. & Hoffmann, M. R., Effect of doped metal ions on the photocatalytic reactivity of TiO₂ quantum particles. *Angew. Chem.* **106**, 1148 (1994).
- Asahi, R., Morikawa, T., Ohwaki, T., Aoki, K. & Taga, Y., Visible-light photocatalysis in nitrogen-doped titanium oxides. *Science* **293**, 269 (2001).
- Khan, S. U. M., Al-Shahry, M. & Ingler, W. B., Efficient photochemical water splitting by a chemically modified n-TiO₂. *Science* **297**, 2243 (2002).
- Chen, X. & Burda, C., The electronic origin of the visible-light absorption properties of C-, N- and S-doped TiO₂ nanomaterials. *J. Am. Chem. Soc.* **130**, 5018 (2008).
- Chen, X. & Burda, C., Photoelectron spectroscopic investigation of nitrogen-doped titania nanoparticles. *J. Phys. Chem. B* **108**, 15446 (2004).
- Zuo, F., Wang, L., Wu, T., Zhang, Z., Borchardt, D., & Feng, P., Self-doped Ti³⁺ enhanced photocatalyst for hydrogen production under visible light, *J. Am. Chem. Soc.* **132**, 11856 (2010).
- Tauc, J., Abraham, A., Pajasova, L., Grigorovici, R., & Vancu, A., *Non-Crystalline Solids* (North-Holland, Amsterdam, 1965).
- Yu, P. Y. & Cardona, M., *Fundamentals of Semiconductors: Physics and Materials Properties*, 4th Ed. (Springer, Heidelberg, 2010).
- Diebold, U., The surface science of titanium dioxide. *Surf. Sci. Rep.* **48**, 53 (2003).
- Thompson, T. L. & Yates, J. T., Surface science studies of the photoactivation of TiO₂ - new photochemical processes. *Chem. Rev.* **106**, 4428 (2006).
- Kudo, A. and Miseki, Y., Heterogeneous photocatalyst materials for water splitting. *Chem. Soc. Rev.* **38**, 253 (2009).
- McCafferty, E. & Wightman, J. P., Determination of the concentration of surface hydroxyl groups on metal oxide films by a quantitative XPS method. *Surf. Interf. Anal.* **26**, 549 (1998).
- Kresse, G. & Hafner, J., *Ab initio* molecular dynamics for liquid metals, *Phys. Rev. B* **47**, 558 (1993).

19. Kresse, G. & Hafner, J., Ab initio molecular dynamics for open-shell transition metals, *Phys. Rev. B* **48**, 13115 (1994).
20. Kresse, G. & Furthmüller, J., Efficiency of ab-initio total energy calculations for metals and semiconductors using a plane-wave basis set, *Comput. Mater. Sci.* **6**, 15 (1996).
21. DiValentin, C., Pacchioni, G., & Selloni, A., Reduced and n-Type Doped TiO₂: Nature of Ti³⁺ Species, *J. Phys. Chem. C* **113**, 20543 (2009).
22. Van de Walle, C. G., Hydrogen as a cause of doping in zinc oxide, *Phys. Rev. Lett.* **85**, 1012 (2000).
23. Kilic, C. & Zunger, A., n-type doping of oxides by hydrogen, *Appl. Phys. Lett.* **81**, 73 (2002).
24. Na-Phattalung, S., et al. First-principles study of native defects in anatase TiO₂, *Phys. Rev. B* **73**, 125205 (2006).
25. Acknowledgements: We thank M. T. Lee and S. H. Shen for their assistance, and R. Greif for discussions and critical reading of the manuscript. This research has been supported by the Office of Energy Efficiency and Renewable Energy of the U. S. Department of Energy. SSM and XC also acknowledge the support from KAUST-UC Academic Excellence Alliance. TEM work was performed at NCEM, which is supported by the Office of Science, Office of Basic Energy Sciences of the U.S. Department of Energy.

Supporting Online Material

www.sciencemag.org/cgi/content/full/science.1200448/DC1

Methods

SOM Text

Figs. S1 to S6

References

15 November 2010; accepted 11 January 2011

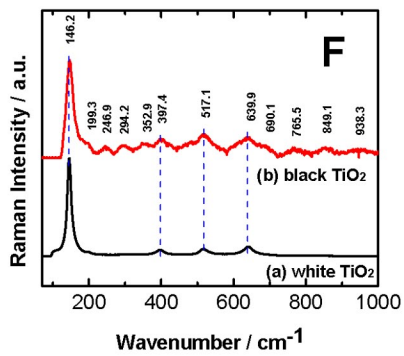
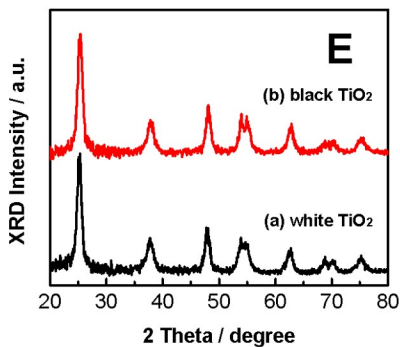
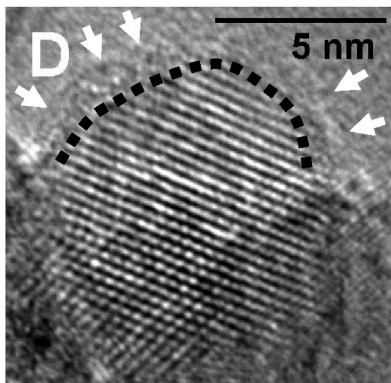
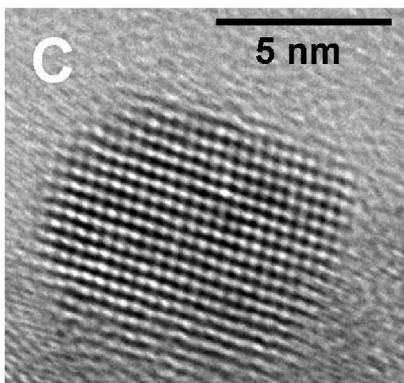
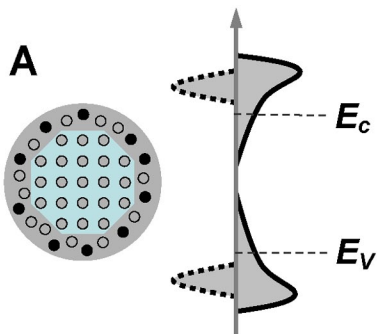
Published online 20 January 2011; 10.1126/science.1200448

Fig. 1. (A) Schematic illustration of the structure and electronic density of states of a semiconductor in the form of a disorder-engineered nanocrystal with dopant incorporation. Dopants are depicted as black dots, and disorder is represented in the outer layer of the nanocrystal. The conduction and valence levels of a bulk semiconductor, E_C and E_V , respectively, are also shown, and the bands of the nanocrystals are shown to the left. The effect of disorder, which crease broadened tails of states extending into the otherwise forbidden band gap, is shown to the right. **(B)** A photo comparing un-modified white and disorder-engineered black TiO₂ nanocrystals. **(C and D)** are HRTEM images of TiO₂ nanocrystals before and after hydrogenation, respectively. In **(D)**, a short-dashed curve is applied to outline a portion of the interface between the crystalline core and the disordered outer layer (marked by white arrows) of black TiO₂. **(E and F)** are XRD and Raman spectra of the white and black TiO₂ nanocrystals.

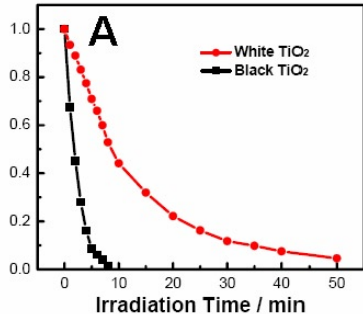
Fig. 2. (A) Comparison of solar-driven photocatalytic activity of the black TiO₂ nanocrystals against that of the white TiO₂ nanocrystals under the same experiment conditions. The y-axis represents the optical density of the methylene blue solution, while the x-axis is the solar light irradiation time. **(B)** Cycling tests of solar-driven photocatalytic activity (methylene blue decomposition) of the disorder-engineered, black TiO₂ nanocrystals. Data in the figure represent the first eight minutes of measurements in each of the eight consecutive photo-degradation testing cycles. **(C)** Cycling measurements of hydrogen gas generation through direct photocatalytic water splitting with disorder-engineered, black TiO₂ nanocrystals under simulated solar light. Experiments were conducted in a 22-day period, with 100 hours of overall solar irradiation time.

Fig. 3. (A) O 1s XPS spectra of the white and black TiO₂ nanocrystals. The red and black circles are XPS data. The green curve is the fitting of experimental data for black TiO₂ nanocrystals, which can be decomposed into superposition of two peaks shown as blue curves. **(B)** Spectral absorbance of the white and black TiO₂ nanocrystals. The inset enlarges the absorption spectrum in the range from approximately 750 nm to 1200 nm. **(C)** Valence band XPS spectra of the white and black TiO₂ nanocrystals. **(D)** Schematic illustration of the density of states of disorder-engineered black TiO₂ nanocrystals, as compared to that of un-modified TiO₂ nanocrystals.

Fig. 4. (A) Schematic illustration of a supercell for modeling disorder-engineered TiO₂ nanocrystal (red: O atoms, gray: Ti atoms, white: H atoms), as compared to a supercell modeling bulk anatase TiO₂. **(B)** Calculated DOS of TiO₂ in the form of a disorder-engineered nanocrystal, an un-modified nanocrystal, and a bulk crystal. The energy of the valence band maximum of the bulk phase is taken to be zero. **(C)** Decomposition of the total DOS of disorder-engineered black TiO₂ nanocrystals into partial DOS of the Ti, O, and H orbitals. **(D)** 3D plot of calculated charge density distribution of a mid-gap electronic state (at about 1.8 eV) of disorder-engineered TiO₂ nanocrystals.



O.D. / a.u.



O.D. / a.u.

